Title: Direct piriform-to-auditory cortical projections shape auditory-olfactory integration

Abbreviated title: Auditory-olfactory integration in auditory cortex

Nathan W. Vogler[1], Ruoyi Chen[1], Alister Virkler[2], Violet Y. Tu[1], Jay A. Gottfried[2], and Maria N. Geffen[1,*]

[1]Department of Otorhinolaryngology, Perelman School of Medicine, University of Pennsylvania

[2]Department of Neurology, Perelman School of Medicine, University of Pennsylvania

*Corresponding Author: mgeffen@pennmedicine.upenn.edu

3450 Hamilton Walk, Stemmler Hall G10, Philadelphia, PA 19104

Number of pages: 42

Number of figures: 6

Number of tables: 1

Number of words: Abstract (163), Introduction (650), Discussion (1066)

Keywords: auditory cortex, piriform cortex, auditory, olfactory, multisensory integration

Conflict of Interest: The authors declare no competing financial interests.

Acknowledgements: Funding: NIH F32MH127788 (to N.W.V.), Kaufman Foundation KA2020-114796 (to M.N.G. and J.A.G.), NIH R01DC015527, NIH R01DC014479, and NIH R01NS113241 (to M.N.G.). The authors would like to thank Tyler Ling for technical assistance.

Abstract

In a real-world environment, the brain must integrate information from multiple sensory modalities, including the auditory and olfactory systems. However, little is known about the neuronal circuits governing how odors influence and modulate sound processing. Here, we investigated the mechanisms underlying auditory-olfactory integration using anatomical, electrophysiological, and optogenetic approaches, focusing on the auditory cortex as a key locus for cross-modal integration. First, retrograde and anterograde viral tracing strategies revealed a direct projection from the piriform cortex to the auditory cortex. Next, using *in vivo* electrophysiological recordings of neuronal activity in the auditory cortex of awake mice, we found that odor stimuli modulate auditory cortical responses to sound. Finally, we used *in vivo* optogenetic manipulations during electrophysiology to demonstrate that olfactory modulation in auditory cortex, specifically, odor-driven enhancement of sound responses, depends on direct input from the piriform cortex. Together, our results identify a novel cortical circuit shaping olfactory modulation in the auditory cortex, shedding new light on the neuronal mechanisms underlying auditory-olfactory integration.

Significance Statement

All living organisms exist within multisensory environments, yet there is a lack in our understanding of how the brain integrates multisensory information. This work elucidates novel circuits governing auditory-olfactory integration in the auditory cortex. Our results shed new light on a relatively understudied area of multisensory research, promising a more robust understanding of how animals and humans perceive and interact within complex environments.

Introduction

A fundamental role of the central nervous system is to integrate information across multiple sensory modalities to optimize decision-making and behavior. Indeed, it is the rare instance that any individual sensory modality operates alone and unabetted: humans and animals must

integrate combinations of sounds, smells, visual input, tactile and proprioceptive information (Gottfried and Dolan, 2003; Deroy et al., 2016; Angeloni and Geffen, 2018; Choi et al., 2018; Wallace et al., 2020). In the specific instance of combining sounds and smells, the brain needs to integrate information from both the auditory and olfactory systems. Auditory-olfactory integration is an ethologically important domain of multisensory integration. When a cat approaches a mouse, the mouse may use the combination of sounds and smell of the cat to identify it as a predator (Halene et al., 2009). Moreover, combinations of auditory and olfactory stimuli are crucial for pup retrieval behavior in mice, and play critical roles during development — bonds between parents and offspring form based on body odors and vocalization sounds (Marlin and Froemke, 2017; Tasaka et al., 2020; McRae et al., 2023). In humans, the sounds of eating food, such as a crunchy potato chip, affect perception of the pleasantness of the food odor, such as potato chip odor/staleness (Seo and Hummel, 2011; Seo et al., 2014). However, the circuits and mechanisms underlying the integration of auditory and olfactory sensory information remain elusive.

Previous studies examining interactions between audition and olfaction have demonstrated cross-modal activation of piriform and auditory cortical areas (Smith et al., 2009; Wesson and Wilson, 2010; Cohen et al., 2011; Varga and Wesson, 2013; Cohen and Mizrahi, 2015; Gnaedinger et al., 2019; Olofsson et al., 2019; Tasaka et al., 2020; Gilday and Mizrahi, 2023; Wu et al., 2023). In the auditory cortex of lactating mother mice, pup odors reduce spontaneous activity and increase evoked activity in response to pup ultrasonic vocalizations (Cohen et al., 2011; Cohen and Mizrahi, 2015). Furthermore, learned associations between an odor and a subsequent sound modulate single-neuron responses in the auditory cortex (Gilday and Mizrahi, 2023). Together, these studies crucially suggest that the auditory cortex (ACx) serves as a locus for auditory-olfactory cross-modal integration, specifically regarding the olfactory modulation of sound processing.

While these studies point to an involvement of the ACx in auditory-olfactory integration, much remains unknown regarding where and how these cross-modal inputs converge. By comparison, previous research on audio-visual integration has found that concurrent visual stimuli improve sound detection and encoding in ACx, facilitated by cross-cortical connections between visual cortex and ACx (Bizley et al., 2016; Atilgan et al., 2018; Meijer et al., 2018; Zhou et al., 2020; Han et al., 2021). Moreover, audio-visual integration crucially depends on the temporal binding of the combined audio-visual stimuli (Meijer et al., 2017, 2019). Similar studies on auditory-olfactory integration have been limited by experimental challenges in delivering combinations of odors and sounds with temporal precision, as well as a lack of knowledge of the brain circuitry underlying auditory-olfactory interactions. Notably, reports of potential cross-modal anatomical connections linking the piriform cortex (Pir) and ACx have been inconsistent. Some have found that ACx projects to Pir but not vice versa (Budinger et al., 2006; Budinger and Scheich, 2009; Wesson and Wilson, 2011), whereas others have reported a sparse but detectable direct projection from Pir to ACx (Costa et al., 2017; Tasaka et al., 2020). Identifying and characterizing these pathways are important first steps in deciphering how the brain integrates auditory and olfactory stimuli.

Here, we confirm the direct Pir-to-ACx projection using multiple circuit tracing strategies and examine its functional role in auditory-olfactory integration in ACx. We explore the impact of this pathway on olfactory modulation of auditory processing, using a novel experimental setup for delivering odors and sound stimuli with temporal precision to awake mice during *in vivo* electrophysiological recordings in ACx. Our findings reveal that the Pir-to-ACx pathway contributes specifically to odor-mediated enhancement of sound responses in ACx.

Materials and Methods

Mice

For anatomical circuit tracing experiments, we used 5 male C57BL/6J mice (The Jackson Laboratory; strain #000664; RRID:IMSR_JAX:000664; aged 8-16 weeks), 2 male Cdh23 mice

105 (B6N(Cg)-Cdh23$^{tm2.1Kjn}$/Kjn; The Jackson Laboratory, strain #:018399; RRID:IMSR_JAX:018399;
106 aged 22 weeks), and 13 Ai14 Cre reporter mice (progeny of Cdh23 mice crossed with Ai14 mice
107 [B6.Cg-Gt(ROSA)$^{26Sortm14(CAG-tdTomato)Hze}$/J; The Jackson Laboratory, strain #:007914;
108 RRID:IMSR_JAX:007914], 7 male, 6 female, aged 18-26 weeks). For electrophysiological
109 recordings, we used 17 mice: 4 C57BL/6J mice (2 male, 2 female; aged 12-17 weeks at time of
110 recording); and 13 Cdh23 mice (5 male, 8 female; aged 12-26 weeks). Mice were housed at 28
111 °C with a 12-h reversed light cycle and food and water provided *ad libitum*. Experiments were
112 performed during the animals' dark cycle. All experimental procedures were approved by the
113 Institutional Care and Use Committee at the University of Pennsylvania and in accordance with
114 National Institutes of Health guidelines.
115
116 *Stereotaxic surgery and virus injections*
117 Mice were anesthetized under isoflurane (1-3%). Prior to surgery, mice were administered
118 subcutaneous doses of buprenorphine (0.05-0.1 mg/kg Buprenex or 1.3 mg/kg Ethiqa),
119 dexamethasone (0.2 mg/kg), and bupivicane (local; 2 mg/kg). A small craniotomy (~1 mm
120 diameter) was made above the respective ACx or Pir injection sites. To label ACx-projecting
121 neurons in Pir in Cdh23 mice, we injected AAVrg-hSyn-eGFP (Addgene #50465-AAVrg;
122 RRID:Addgene_50465; 250 nL) into left ACx (4.3 mm ML and -2.65 mm AP [relative to Bregma],
123 -0.7 mm DV [relative to brain surface]). To label ACx-projecting neurons in Pir in Ai14 mice, we
124 injected AAVrg-hSyn-Cre-WPRE-hGH (Addgene #105553-AAVrg; RRID:Addgene_105553; 150-
125 250 nL) into left ACx. To label Pir-recipient neurons in ACx in Ai14 mice, we injected AAV1-hSyn-
126 Cre-WPRE-hGH (Addgene #105553-AAV1; RRID:Addgene_105553; 150-180 nL) into left Pir (3.9
127 mm ML, -1.5 mm AP, -4.00 DV). Viruses were delivered through 30-40 μm diameter glass
128 micropipettes connected to a syringe pump (Harvard Apparatus Pump 11 Elite; 60 nL/min infusion
129 rate). For optogenetic experiments, in Cdh23 or C57BL/6J mice we injected AAVrg-hSyn-Cre-

130 WPRE-hGH (300 nL) into left ACx and AAV5-hSyn1-SIO-stGtACR1-FusionRed (Addgene
131 #105678-AAV5; RRID:Addgene_105678; 300 nL) or AAV5-FLEX-tdTomato (Addgene #28306-
132 AAV5; RRID:Addgene_28306; 300 nL) into left Pir (3.9 mm ML, -1.0 mm AP, -4.00 mm DV). A
133 fiber optic cannula (ThorLabs CFML52L05; Ø200 µm Core, 0.50 NA, L=5mm) was implanted over
134 left Pir (3.9 mm ML, -1.0 mm AP, -3.6 mm DV) and secured with dental cement (C&B Metabond).
135 For all electrophysiological recordings, a ground pin was inserted via small craniotomy over the
136 left frontal cortex, and a custom-made stainless steel headplate (eMachine Shop) was secured to
137 the skull using dental cement and acrylic (Lang Dental). After all surgeries, we subcutaneously
138 administered meloxicam (5 mg/kg) and an antibiotic (Baytril 5 mg/kg) for 4 days during
139 postoperative care. After virus injections, to allow adequate time for virus expression, we waited
140 at least two weeks (for retrograde tracing/optogenetics) or three weeks (for anterograde tracing)
141 before subsequent recording and/or transcardial perfusion.
142
143 *Histology and cell counting*
144 Mice were anesthetized via intraperitoneal injection of ketamine (120 mg/kg) and
145 dexmedetomidine (1 mg/kg), then perfused with phosphate-buffered saline (PBS) followed by 4%
146 paraformaldehyde (PFA) in PBS. Brains were extracted and immersed in 4% PFA overnight then
147 in 30% sucrose in PBS for at least 36 hours at 4°C. Coronal brain sections (60 µm thickness)
148 were cut on a cryostat (Leica CM1860) at -25°C and mounted on slides using Invitrogen ProLong
149 Antifade Mountant with DAPI. Fluorescent images were acquired using a slide scanning
150 microscope (Zeiss Axio Scan.Z1) under 20x magnification and ZEN 2.3 software. Whole brain
151 fluorescent images were manually aligned with the reference mouse brain atlas (Franklin &
152 Paxinos) to determine regions of interest (ROIs) for cell counting. For the anterior Pir, four coronal
153 sections between 1.0-2.0 mm anterior to Bregma were counted in each mouse. For the posterior
154 Pir, four coronal sections between 1.5-2.5 mm posterior to bregma were counted in each mouse.

155 Fluorescent-labeled cells within ROIs were manually counted using ImageJ software. For ACx
156 subregions, eight coronal sections between 2.2-3.6 mm posterior to bregma were counted in each
157 mouse. A custom-written MATLAB script was used to register the normalized depth of each cell
158 from the pia during manual counting. Specifically, for each ACx subregion, a line segment
159 spanning the depth of the cortex was drawn perpendicular to the pia in the middle of the
160 subregion. The normalized depth for each cell was defined as the relative length of the projection
161 of the cell's location onto that line segment.
162
163 *Electrophysiological recordings*
164 Recordings were performed in a custom-built acoustic isolation booth. At least one week following
165 headplate surgery, mice were habituated to the recording setup for increasing durations (5 – 60
166 min) over the course of 3 days. On the day of recording, mice were anesthetized with 1.5-2.5%
167 isoflurane, and a small craniotomy was made over the left auditory cortex using a dental drill,
168 centered ~1.5mm anterior to the lambdoid suture along the caudal end of the squamosal suture.
169 Following the craniotomy, mice were allowed to recover from anesthesia for at least 30 min. Acute
170 extracellular recordings in ACx were performed using a 32-channel silicon probe (A1x32-Poly2-
171 5mm-50s-177, NeuroNexus). Prior to insertion, the probe was coated in a dye (CM-DiI or SP-DiO;
172 Invitrogen) for post hoc visualization of recording sites. The probe was positioned perpendicularly
173 to the brain surface and lowered at 1-2 μm/s to a final depth of 900-1200 μm or until all channels
174 were within the brain. During lowering of the probe, we monitored responses to brief broadband
175 noise clicks to confirm localization within auditory cortex. Neuronal signals were amplified and
176 digitized with an Intan headstage (RHD 32ch) and recorded by an OpenEphys acquisition board
177 (Siegle et al., 2017) at a rate of 30 kHz. Signals were filtered between 500 and 6000 Hz, offset
178 corrected, and re-referenced to the median across all channels. Spiking data were sorted using
179 Kilosort2 (Pachitariu et al., 2016) and manually curated in phy2 to identify putative single- and
180 multi-units.

181

182 *Stimuli*

183 Stimuli during electrophysiological recordings consisted of combinations of auditory and olfactory
184 stimuli. Odor stimuli consisted of Acetophenone (CAS 98-86-2; Sigma-Aldrich), Eucalyptus (100%
185 pure eucalyptus oil; NOW essential oils), or an Acetophenone + Eucalyptus mixture (1:1 vol/vol),
186 delivered using a respiration-triggered flow dilution olfactometer (Shusterman et al., 2011; Dewan
187 et al., 2018; Williams and Dewan, 2020). Odorants were liquid diluted 1:1 vol/vol in mineral oil
188 (CAS 8042-47-5; Sigma-Aldrich) in amber vials, then further air diluted (2% N_2/Air) in the
189 olfactometer, for a final dilution of 1%. The control (non-odorant) vial contained pure mineral oil.
190 The olfactometer and stimulus delivery were controlled by custom Python software and Arduino
191 MEGA 2560. Throughout the recording, we monitored the respiratory cycle of the mouse.
192 Between each trial, the olfactometer tubing was cleared and primed with the next odor for at least
193 3 s. At the onset of a trial, the mouse's inhale triggered the 'final valve' to switch from delivering
194 continuous clean background air to odorized air, which rapidly delivered the odorized air to the
195 mouse's nose with no change in total air flow (valve opening duration 1.25 s). Opening of the final
196 valve also triggered playing of the sound stimulus with a delay of 250 ms to allow adequate time
197 for the odor to reach the mouse's nose and subsequent inhale. The onset timing and kinetics of
198 odor stimuli were verified using a photo-ionization detector (miniPID; Aurora Scientific). Sounds
199 consisted of 1 s duration broadband gaussian white noise filtered between 3-60 kHz, either
200 unmodulated or amplitude-modulated (10 Hz, 100% modulation depth). Sounds were generated
201 in Python and converted to analog signals via National Instruments card (NI PCIe-6353, 200 kHz
202 sample rate) and delivered through a speaker (MF-1; Tucker-Davis Technologies) pointed toward
203 the mouse's right ear, at 0, 45, 55, 65, or 75 dB SPL. Background noise from the olfactometer air
204 flow was measured to be ~50 dB SPL (1/4-inch condenser microphone; Brüel &Kjær). During
205 recordings, on half of trials, we delivered either odorized air or control air. For recordings with
206 optogenetics, on half of trials, we delivered 470 nm LED light (M470F4; ThorLabs) through a fiber

optic cannula (ThorLabs CFML52L05; power 2.8-3.7 mW at cannula tip). LED stimulus onset and duration (1.25 s) were the same as final valve opening. For all recordings, trial order was randomized and different for each recording.

Electrophysiological data analysis

Neuronal spiking data from each recorded unit were organized by trial type and aligned to the trial onset (i.e. the time of final valve opening). For each unit, peristimulus time histograms (PSTHs) of neuronal spikes were generated using 10 ms time bins, then averaged across trials for each condition. We included all units with baseline firing rate > 1 Hz. For responses to unmodulated noise stimuli, we analyzed spiking during a response window of 0-250 ms after sound onset; for responses to 10 Hz AM stimuli, we analyzed spiking during a response window of 0-1 s. To classify each unit as sound-responsive or odor-modulated, we input the number of spikes during each trial's response window into a generalized linear model (GLM; predictor variables: sound level [continuous variable normalized from 0-1], odor [0 or 1]; response variable: number of spikes during response window; Poisson distribution, log link function). This allowed the classification of each unit's responses as having a main effect (p<0.05) of sound, odor, and/or a sound-odor interaction. Sound-responsive units that were also responsive to odor or had a significant sound-odor interaction were classified as 'odor-modulated' units. For each odor-modulated unit, to determine the direction and magnitude of olfactory modulation, we calculated an Odor Modulation Index (OMI) according to:

$$OMI = \frac{FR_{Odor} - FR_{Air}}{FR_{Odor} + FR_{Air}}$$

Where FR_{Odor} and FR_{Air} are the mean firing rates in response to sound, with or without odor, respectively. For each unit we calculated the OMI using the mean firing rates for all responses to 5, 15, and 25 dB SNR sounds. Odor-modulated units with OMI>0 were classified as 'enhanced' units; units with OMI<0 were classified as 'suppressed' units. In addition, for both enhanced and

232 suppressed units, we calculated the OMI for each sound level using the responses to each sound
233 stimulus separately. To calculate z-scored firing rates, we used the mean and standard deviation
234 across trials of firing rate during the 1 s baseline period prior to final valve opening. For 'enhanced'
235 units in optogenetics experiments (stGtACR1 and control mice), we calculated an LED Modulation
236 Index according to:

237 $$LED\ Modulation\ Index = \frac{FR_{Odor\ (LED\ ON)} - FR_{Odor\ (LED\ off)}}{FR_{Odor\ (LED\ ON)} + FR_{Odor\ (LED\ off)}}$$

238 Where $FR_{Odor\ (LED\ ON)}$ and $FR_{Odor\ (LED\ off)}$ are the mean firing rates in response to Odor+Sound, with
239 or without LED light, respectively.
240
241 *Statistics*
242 Data analysis and figure generation were performed using Matlab or Python. We used the
243 Shapiro-Wilk test to assess normality. For parametric data we used two-tailed paired or unpaired
244 t-tests between groups; for non-parametric data we used two-tailed Wilcoxon signed-rank or
245 Mann-Whitney tests between groups, or Friedman tests for multiple groups. We performed
246 Bonferroni corrections for multiple comparisons. Significance levels are defined as $p<0.05$. Group
247 data in figures are presented as mean ± SEM, unless otherwise noted. The statistical tests
248 performed are indicated in the text and figure legends. Table 1 contains a detailed summary of
249 statistical tests and comparisons.
250
251 *Data and code availability*
252 Source data is available on Dryad: https://doi.org/10.5061/dryad.dncjsxm7c . Original code is
253 available on GitHub: https://github.com/geffenlab/Vogler_2024.
254
255 **Results**
256 **The auditory cortex receives direct input from the piriform cortex.**

257 To examine potential anatomical substrates for auditory-olfactory integration in the auditory cortex
258 (ACx), we first sought to identify whether ACx receives direct projections from olfactory brain
259 areas such as the piriform cortex (Pir). We started by injecting a retrograde virus expressing GFP
260 (AAVrg-hSyn-eGFP) into the left ACx to selectively label the cell bodies of ACx-projecting neurons
261 (Fig. 1A). We observed fluorescently labeled cells in the ipsilateral Pir (GFP, Fig. 1B). Because
262 the anterior and posterior regions of the Pir are known to exhibit differential long-range
263 connectivity patterns (Bekkers and Suzuki, 2013), we quantified and compared retrograde GFP
264 expression in the anterior Pir (aPir) versus posterior Pir (pPir) (Fig. 1B-C). In most mice, we
265 observed a greater number of labeled cells in pPir compared to aPir. (Fig. 1C), suggesting that
266 the Pir-to-ACx projection predominantly arises from pPir. To further confirm the existence of this
267 projection and validate our approach, we performed a similar retrograde tracing experiment in
268 Ai14 cre-reporter mice, injecting retroAAV expressing Cre (AAVrg-hSyn-Cre) into the ACx (Fig.
269 1D). Again, we found retrogradely labeled cell bodies in ipsilateral Pir (tdTomato, Fig. 1E), and we
270 observed a significantly greater number of labeled cells in pPir compared to aPir (Fig. 1F,
271 *p=0.020, paired t-test). These retrograde tracing experiments reveal a direct projection to ACx
272 arising from Pir, predominantly from pPir.
273
274 Next, to further characterize Pir input to ACx, we performed anterograde viral tracing to reveal the
275 targets of Pir neurons within ACx. We injected a transsynaptic anterograde virus (Zingg et al.,
276 2020) expressing Cre (AAV1-hSyn-Cre) into the left Pir of Ai14 mice to selectively label neurons
277 in ACx that receive Pir input (Fig. 2A). Because our retrograde tracing experiments (Fig. 1)
278 showed that the Pir-to-ACx projection arises mostly from pPir, we specifically targeted pPir for the
279 anterograde virus injections. Consistent with our retrograde tracing experiments, we observed
280 fluorescently labeled cell bodies in the ipsilateral ACx, including the primary ACx (Au1) and the
281 dorsal and ventral secondary ACx (AuD, AuV) (Fig. 2B-C). We additionally observed Pir-recipient
282 cells in the temporal association cortex (TeA) (Fig. 2B-C), consistent with previous studies (Tasaka

283 et al., 2020). We quantified and compared anterograde tdTomato expression across these cortical
284 subregions and found an increase in the number of labeled cells from dorsal-to-ventral auditory
285 subregions (Fig. 2C, *p=0.014, Friedman test). Furthermore, we quantified the cortical depth of
286 the labeled cells, and found that Pir-recipient cells span all layers of ACx, but predominantly in
287 layers 2/3 and 6 (Fig. 2D). These anterograde tracing experiments further confirm the direct
288 projection from Pir to ACx and reveal that Pir-recipient ACx neurons span auditory cortical and
289 layers and subregions.
290
291 Taken together, our tracing experiments identify a direct projection from pPir to ACx using multiple
292 retrograde and anterograde viral approaches. These results suggest an anatomical substrate by
293 which olfactory sensory information may affect auditory processing in ACx, pointing toward a
294 possible mechanism for auditory-olfactory integration.
295
296 ***In vivo* electrophysiology for assessing auditory-olfactory integration in auditory cortex.**
297 Next, we sought to determine whether and how odors modulate auditory processing in the ACx
298 of awake mice. While previous studies have demonstrated olfactory modulation of sound
299 responses in ACx, most of these studies were performed in anesthetized animals using complex
300 odorants and sound stimuli, or in awake animals but influenced by a behavioral task (Cohen et
301 al., 2011; Cohen and Mizrahi, 2015; Gnaedinger et al., 2019; Gilday and Mizrahi, 2023). We
302 therefore sought to answer the basic question of whether and how a temporally coupled odor
303 modulates ACx responses to simple sounds in untrained, awake mice. To answer this question,
304 we designed a custom-made system combining sound stimuli with a respiration-triggered
305 olfactometer to deliver sounds and odors to awake head-fixed mice with high temporal precision
306 during *in vivo* electrophysiology (Fig. 3A). We recorded the activity of ACx neurons in response
307 to combinations of odor (Acetophenone or Eucalyptus, 1%) and sound stimuli (unmodulated or
308 amplitude-modulated [AM, 10 Hz] noise, 0 – 75 dB). We used the respiration-triggered

309 olfactometer to control the timing of odor/sound stimulus delivery with the mouse's inhale (Fig.
310 3B). To examine auditory-olfactory integration in ACx, we targeted recordings to the ACx (Fig. 3C)
311 and recorded the activity of single- and multi-units in response to sounds, with or without odor
312 (Fig. 3D).
313
314 Because our anatomical experiments pointed toward the Pir-to-ACx pathway as a possible
315 substrate for auditory-olfactory integration in ACx, we tested whether and how this pathway
316 contributes to odor modulation of sound responses using an *in vivo* optogenetic approach. To
317 selectively inactivate ACx-projecting Pir neurons, we injected AAVrg-hSyn-Cre into ACx, and the
318 cre-dependent soma-targeted inhibitory opsin stGtACR1 (AAV5-SIO-stGtACR1) (Mahn et al.,
319 2018) into pPir (Fig. 3E). During *in vivo* recordings, we delivered 470 nm LED light through a fiber
320 optic cannula implanted over pPir (Fig. 3E-F). Fig. 3G-H shows sound responses in an example
321 ACx unit under the various trial conditions: odor enhances the sound responses, but this
322 enhancement is eliminated by LED inactivation of ACx-projecting Pir neurons.
323
324 **Odor modulates sound responses in auditory cortex.**
325 First, we tested whether and how odors modulate sound stimuli in ACx. We identified 'sound-
326 responsive' and 'odor-modulated' units using a generalized linear model (GLM). In response to
327 unmodulated broadband noise, ~20% of sound-responsive units were significantly modulated by
328 odor (Fig. 4A). However, the effects of the odor on sound responses were heterogenous: in
329 response to unmodulated noise, we observed both enhancement (Fig. 4B, left) and suppression
330 (Fig. 4B, right) of sound responses by odor. To quantify the amount of enhancement or
331 suppression in odor-modulated units, we calculated an Odor Modulation Index (OMI) for each unit
332 for each sound level (Fig. 4C). We found that OMIs vary significantly across sound level for
333 enhanced units (Fig. 4C, left; *p=0.039, Friedman test), but not suppressed units (Fig. 4C, right;
334 n.s. p=0.326, Friedman test). In addition, we tested the effect of odor on responses to 10 Hz

amplitude-modulated (AM) noise and performed the same analyses (Fig. 4E-H). In response to AM noise, we found a greater proportion of odor-modulated sound-responsive units (~33%, Fig. 4E). We again observed both enhancement and suppression of sound responses by odor (Fig. 4F), and that OMIs vary significantly across sound level for enhanced units (Fig. 4G, left; *p=0.028, Friedman test).

Furthermore, in sound-responsive odor-modulated units, we tested the effect of odor on neuronal firing in the absence of sound. We found that odor significantly enhanced neuronal firing rate, compared to control (Fig. 4I, **p=0.0042, Wilcoxon signed-rank test). This result suggests that odor stimuli impact ACx processing in the absence of sound, as well as in response to sound stimuli. Specifically, odor stimuli enhance baseline neuronal firing, but either enhance or suppress sound-evoked responses.

Together, these results demonstrate that: 1) olfactory stimuli modulate auditory processing in awake mice, including enhancement of baseline firing as well as bidirectional modulation of sound-evoked responses; and 2) olfactory stimuli enhance or suppress neuronal responses to multiple types of sound stimuli, including both unmodulated and AM noise.

Piriform input to auditory cortex contributes to auditory-olfactory integration.

To test the role of the newly characterized Pir-to-ACx pathway (Fig. 1-2) in auditory-olfactory olfactory integration, we combined *in vivo* electrophysiology in awake mice with optogenetics specifically targeting ACx-projecting Pir neurons (Fig. 3). We again recorded sound responses with or without odor, but now we also optogenetically inactivated ACx-projecting Pir neurons by shining LED light through a cannula implanted over ipsilateral pPir (Fig. 3E-H). Consistent with our previous experiments (Fig. 4), we observed both enhancement and suppression of sound responses by odor in a subpopulation of ACx units (Fig. 5A). For both the enhanced and

361 suppressed units, we compared the amount of odor modulation, using the OMI, with or without
362 LED-inactivation of Pir neurons. Strikingly, we observed that for the enhanced units, the LED
363 significantly reduced odor modulation (**p=0.001, Wilcoxon signed-rank test), whereas odor
364 modulation in suppressed units was unaffected (n.s. p=0.96, Wilcoxon signed-rank test) (Fig. 5A).
365 We then examined the effect of the LED on odor modulation for each sound level (Fig. 5B-C) and
366 found that in enhanced units, the LED significantly reduced the amount of odor modulation (OMI)
367 at the highest sound level (Fig. 5C, left; 25 dB SNR: *p=0.042, Wilcoxon signed-rank test),
368 whereas in suppressed units the odor modulation was unaffected (Fig. 5C, right; 25 dB SNR: n.s.
369 p=0.73, Wilcoxon signed-rank test). We again repeated the same analyses for responses to AM
370 noise and observed similar results: the LED significantly reduced the amount of odor modulation
371 in enhanced units (**p=0.004, Wilcoxon signed-rank test), but not in suppressed units (n.s.
372 p=0.63, Wilcoxon signed-rank test) (Fig. 5E). For enhanced units, the LED significantly reduced
373 the amount of odor modulation at 15 dB SNR and 25 dB SNR (Fig. 5G, left; 15 dB SNR: *p=0.013;
374 25 dB SNR: *p=0.021; Wilcoxon signed-rank tests), whereas suppressed units were unaffected
375 (Fig. 5G, right; 15 dB SNR: n.s. p=0.10, Wilcoxon signed-rank test; 25 dB SNR: n.s. p=0.23,
376 paired t-test). These results demonstrate that odor *enhancement* of sound responses, but not
377 odor suppression, requires the Pir-to-ACx pathway, suggesting that this pathway provides an
378 excitatory drive.
379
380 Finally, we examined odor-driven enhancement of ACx neuronal firing in the absence of sound,
381 with or without *in vivo* optogenetic inactivation of Pir neurons. Consistent with our previous
382 experiments (Fig. 4I), in odor-modulated ACx units we observed that odor significantly enhanced
383 neuronal firing rate, compared to control (Fig. 5I, left; LED off: ***p=3.07e-7, paired t-test).
384 Strikingly, however, this enhancement was eliminated by the LED (Fig. 5I, left; LED ON, n.s. p>1,
385 Wilcoxon signed-rank test). When comparing the amount of odor modulation (OMI) with versus
386 without the LED, we found that the LED significantly reduced the odor-driven enhancement in the

absence of sound (Fig. 5I, middle; ***p=2.3e-7, Wilcoxon signed-rank test). This result suggests that optogenetic inactivation of ACx-projecting Pir neurons eliminates odor-driven enhancement of baseline ACx neuronal firing, and therefore that this enhancement requires the direct Pir-to-ACx pathway.

Importantly, we performed control experiments to confirm that the optogenetic effects we observed (Fig. 5) were specifically due to inactivation of Pir-to-ACx input via light activation of stGtACR1, and not potential non-specific effects of the LED light. Control mice underwent an identical experimental procedure as the optogenetic mice, except we injected a control virus into Pir (AAV5-Flex-tdTomato) instead of opsin (Fig. 6A). In control mice, LED light did not significantly reduce odor modulation in enhanced units, for both unmodulated noise (Fig. 6B-C, left; n.s. p=0.173, Wilcoxon signed-rank test) and AM noise (Fig. 6B-C, right; n.s. 0.115, Wilcoxon signed-rank test). Next, we examined the effect of the LED on enhanced units in the controls. To quantify the effect of the LED on olfactory modulation, we calculated an LED Modulation Index (Fig. 6E). For both unmodulated noise (Fig. 6E, left; **p=0.01, Wilcoxon signed-rank test) and AM noise (Fig. 6E, right; *p=0.037, Wilcoxon signed-rank test), the LED significantly reduced odor modulation in mice expressing stGtACR1 as compared to controls.

In control mice we again observed odor-driven enhancement of baseline neuronal firing in the absence of sound (Fig. 6F, left; LED off, ***p=8.7e-9, paired t-test); however, this enhancement persisted with the LED (Fig. 6F, left; LED ON, ***p=1.64e-6, Wilcoxon signed-rank test). When comparing the amount of odor modulation (OMI) with versus without the LED, we found that the LED did not affect the odor-driven enhancement in the absence of sound (Fig. 6F, right; n.s. p=0.31, Wilcoxon signed-rank test). These results confirm that the reduction of odor-driven enhancement we observed in mice expressing stGtACR1 (Fig. 5) was specifically due to inactivation of the Pir-to-ACx pathway.

Together, our results identify the role of the Pir-to-ACx pathway in auditory-olfactory integration. Optogenetic inactivation of ACx-projecting Pir neurons selectively reduced odor-driven enhancement of baseline ACx firing as well as enhancement of sound-evoked responses. Therefore, the Pir-to-ACx pathway contributes to odor-mediated enhancement of sound responses, but not suppression.

Discussion

In this study we tested the functional role of a direct projection from the piriform cortex to the auditory cortex. We identified the Pir-to-ACx pathway using retrograde and anterograde viral tracing, highlighting that this pathway arises primarily from posterior Pir (Fig. 1), and projects to multiple ACx subregions and laminae (Fig. 2). Next, using *in vivo* electrophysiology in ACx, we demonstrated that olfactory stimuli directly activate ACx neurons and bidirectionally modulate sound-evoked activity, either enhancing or suppressing sound responses (Figs. 3-4). Finally, using *in vivo* optogenetics during electrophysiology, we found that the Pir-to-ACx projection is necessary for odor-mediated ACx activation and enhancement of sound responses, but is minimally engaged during suppression (Figs 5-6). Our results reveal that the Pir-to-ACx pathway shapes auditory-olfactory integration in ACx, playing a crucial role in odor-mediated *enhancement* of sound processing.

Our anatomical results demonstrate that the Pir-to-ACx projection primarily arises from posterior Pir (pPir), and projects across multiple ACx subregions and cortical layers. Its origination in pPir is consistent with previous studies showing that pPir contains more associational connections with other higher-order brain areas compared to anterior Pir (Bekkers and Suzuki, 2013). For example, pPir is known to have interconnections with the prefrontal cortex, amygdala, and entorhinal and perirhinal cortices, and is thought to encode odor quality (Johnson et al., 2000;

439 Zelano et al., 2011). Our results add ACx to the list of Pir-recipient regions and expand knowledge
440 of cross-modal cortical circuitry. Moreover, the distribution of Pir-recipient neurons spanning ACx
441 is consistent with previous studies showing that cortico-cortical intra-telencephalic neurons
442 project to/from multiple cortical layers including L2/3 and L6 (Shepherd, 2013; Harris and
443 Shepherd, 2015).
444
445 Notably, while previous studies have shown evidence for the Pir-to-ACx projection (Costa et al.,
446 2017; Tasaka et al., 2020), such findings have gone relatively underexplored. Our results are
447 consistent with these previous studies and provide comprehensive evidence for the existence and
448 functional impact of the Pir-to-ACx cross-cortical circuit. We revealed this circuity using a rigorous
449 approach comprised of four different viral strategies: retroAAV-GFP (Fig. 1), retroAAV-Cre (Fig 1),
450 AAV1-Cre (Fig 2), and selective labeling of ACx-projecting Pir neurons for optogenetics (retroAAV-
451 Cre and AAV5-stGtACR1, Fig. 3). Although our experiments yielded robust and reproducible
452 results using these strategies, the question remains why other research groups previously failed
453 to observe this projection. One explanation could simply relate to differences in the tracer used
454 and/or the animal model, e.g., retroAAVs in mice (the present study) versus fluorescein-labeled
455 dextran in gerbils (Budinger et al., 2006; Budinger and Scheich, 2009). In addition, it is quite likely
456 that this pathway may have gone unnoticed in previous studies in which it was not the target of
457 investigation.
458
459 Although there have been a few previous studies examining auditory-olfactory integration in ACx,
460 our data underscore modulation of sound responses by odors in naïve, passively exposed, awake
461 mice. Previous experiments using more complex stimuli, such as modulation of ACx responses
462 to pup vocalizations by pup odors, used acetophenone as a control odor stimulus, showing no
463 effect on sound responses (Cohen et al., 2011). That said, the Cohen et al. study was performed
464 in anesthetized animals, and it has since been well-established that neuronal responses vary

465 greatly in anesthetized versus awake states (Fontanini and Katz, 2008; Lesicko et al., 2022).
466 Furthermore, the combined olfactory and auditory stimuli in previous studies were not bound
467 precisely in time, and often involved other factors such as behavioral training and associative
468 learning that could have altered cross-modal coding (Cohen et al., 2011; Cohen and Mizrahi,
469 2015; Gilday and Mizrahi, 2023). Interestingly, an important recent study has suggested that
470 auditory-olfactory integration occurs in higher-order areas of entorhinal cortex due to shared
471 auditory and olfactory inputs (Wu et al., 2023). Our results add to this growing body of literature
472 and suggest that auditory-olfactory integration occurs at even earlier stages in the sensory
473 processing hierarchy than previously realized.
474
475 Importantly, in sound-responsive odor-modulated units, we found that odor stimuli alone excite
476 these units even in the absence of sound (Figs 4I, 5I, 6F). Thus, olfactory input appears to serve
477 as both a direct activator of ACx as well as a modulator of auditory processing. Our findings of
478 both enhanced and suppressed sound-evoked responses are consistent with previous studies in
479 other modalities such as in audio-visual integration, showing that visual stimuli evoke both
480 excitation and modulation of ACx (Bizley et al., 2007; Kayser et al., 2008; Atilgan et al., 2018).
481
482 We found that Pir input to ACx contributes to odor-driven enhancement of baseline and sound-
483 evoked responses, but not suppression of sound-evoked responses. It is intriguing to consider
484 what mechanism might account for this dichotomy. Because most long-range intra-telencephalic
485 projections are excitatory (Shepherd, 2013; Harris and Shepherd, 2015), odor enhancement may
486 be due to excitation of ACx by direct Pir input, whereas odor suppression may arise from indirect
487 input via local circuitry or via other brain regions. In our anterograde tracing experiments
488 identifying Pir-recipient neurons, we observed that the TeA receives a large amount of Pir input
489 (Fig 2), a finding that is consistent with previous studies (Tasaka et al., 2020, 2023) and suggests
490 that TeA is a region that might relay Pir input to ACx, ultimately affecting ACx activity. Together

these results pave the way for future studies to disentangle the relative contributions of direct Pir input versus indirect pathways to auditory-olfactory integration in ACx, and how the Pir-to-ACx pathway interacts with other multimodal and higher-order brain circuity.

Finally, it is worth noting that previous studies of auditory-olfactory integration have largely focused on parental behavior, including the effects of pup odors on auditory processing in maternal mice, as well as pup retrieval (Cohen and Mizrahi, 2015; Marlin et al., 2015; Marlin and Froemke, 2017; McRae et al., 2023). Moving forward, it will be interesting to determine the extent to which the Pir-to-ACx pathway contributes to more “real-world” behaviors. Although our present study has focused on the effects of simple neutral odorants, future studies are poised to investigate the additional effects of ethologically relevant odor stimuli, such as pup odors, social odors, food odors, or predator odors. Furthermore, auditory-olfactory integration in ACx is known to undergo plasticity during motherhood as well as during formation of odor-sound associations (Cohen and Mizrahi, 2015; Gnaedinger et al., 2019; Gilday and Mizrahi, 2023). Drawing from these findings, we suggest that the Pir-to-ACx pathway serves as a novel contributor to multimodal processing that may play a pivotal role in multisensory plasticity and learning.

References

Angeloni C, Geffen MN (2018) Contextual modulation of sound processing in the auditory cortex. Curr Opin Neurobiol 49:8–15 Available at: www.sciencedirect.comwww.sciencedirect.com [Accessed November 18, 2020].

Atilgan H, Town SM, Wood KC, Jones GP, Maddox RK, Lee AKC, Bizley JK (2018) Integration of Visual Information in Auditory Cortex Promotes Auditory Scene Analysis through Multisensory Binding. Neuron 97:640-655.e4 Available at: https://doi.org/10.1016/j.neuron.2017.12.034 [Accessed December 7, 2020].

Bekkers JM, Suzuki N (2013) Neurons and circuits for odor processing in the piriform cortex.

517 Trends Neurosci 36:429–438.
518 Bizley JK, Jones GP, Town SM (2016) Where are multisensory signals combined for perceptual
519 decision-making? Curr Opin Neurobiol 40:31–37 Available at:
520 http://dx.doi.org/10.1016/j.conb.2016.06.003 [Accessed November 18, 2020].
521 Bizley JK, Nodal FR, Bajo VM, Nelken I, King AJ (2007) Physiological and anatomical evidence
522 for multisensory interactions in auditory cortex. Cereb Cortex 17:2172–2189.
523 Budinger E, Heil P, Hess A, Scheich H (2006) Multisensory processing via early cortical stages:
524 Connections of the primary auditory cortical field with other sensory systems. Neuroscience
525 143:1065–1083.
526 Budinger E, Scheich H (2009) Anatomical connections suitable for the direct processing of
527 neuronal information of different modalities via the rodent primary auditory cortex. Hear
528 Res 258:16–27.
529 Choi I, Lee JY, Lee SH (2018) Bottom-up and top-down modulation of multisensory integration.
530 Curr Opin Neurobiol 52:115–122 Available at: https://doi.org/10.1016/j.conb.2018.05.002.
531 Cohen L, Mizrahi A (2015) Plasticity during motherhood: Changes in excitatory and inhibitory
532 layer 2/3 neurons in auditory cortex. J Neurosci 35:1806–1815.
533 Cohen L, Rothschild G, Mizrahi A (2011) Multisensory integration of natural odors and sounds in
534 the auditory cortex. Neuron 72:357–369.
535 Costa NM da, Martin KAC, Sägesser FD (2017) A weighted graph of the projections to mouse
536 auditory cortex. bioRxiv:228726.
537 Deroy O, Faivre N, Lunghi C, Spence C, Aller M, Noppeney U (2016) The Complex Interplay
538 between Multisensory Integration and Perceptual Awareness. Multisens Res 29:585–606.
539 Dewan A, Cichy A, Zhang J, Miguel K, Feinstein P, Rinberg D, Bozza T (2018) Single olfactory
540 receptors set odor detection thresholds. Nat Commun 9:1–12 Available at:
541 http://dx.doi.org/10.1038/s41467-018-05129-0.
542 Fontanini A, Katz DB (2008) Behavioral states, network states, and sensory response variability.

543 J Neurophysiol 100:1160–1168.
544 Gilday OD, Mizrahi A (2023) Learning-Induced Odor Modulation of Neuronal Activity in Auditory
545 Cortex. J Neurosci 43:1375–1386.
546 Gnaedinger A, Gurden H, Gourévitch B, Martin C (2019) Multisensory learning between odor
547 and sound enhances beta oscillations. Sci Rep 9:11236.
548 Gottfried JA, Dolan RJ (2003) The nose smells what the eye sees: Crossmodal visual facilitation
549 of human olfactory perception. Neuron 39:375–386.
550 Halene TB, Talmud J, Jonak GJ, Schneider F, Siegel SJ (2009) Predator odor modulates
551 auditory event-related potentials in mice. Neuroreport 20:1260–1264.
552 Han X, Xu J, Chang S, Keniston L, Yu L (2021) Multisensory-Guided Associative Learning
553 Enhances Multisensory Representation in Primary Auditory Cortex. Cereb Cortex:1–15.
554 Harris KD, Shepherd GMG (2015) The neocortical circuit: Themes and variations. Nat Neurosci
555 18:170–181.
556 Johnson DMG, Illig KR, Behan M, Haberly LB (2000) New features of connectivity in piriform
557 cortex visualized by intracellular injection of pyramidal cells suggest that “primary” olfactory
558 cortex functions like “association” cortex in other sensory systems. J Neurosci 20:6974–
559 6982.
560 Kayser C, Petkov CI, Logothetis NK (2008) Visual modulation of neurons in auditory cortex.
561 Cereb Cortex 18:1560–1574.
562 Lesicko AMH, Angeloni CF, Blackwell JM, De Biasi M, Geffen MN (2022) Cortico-Fugal
563 Regulation of Predictive Coding. Elife 11:1–29.
564 Mahn M, Gibor L, Patil P, Cohen-Kashi Malina K, Oring S, Printz Y, Levy R, Lampl I, Yizhar O
565 (2018) High-efficiency optogenetic silencing with soma-targeted anion-conducting
566 channelrhodopsins. Nat Commun 9 Available at: http://dx.doi.org/10.1038/s41467-018-
567 06511-8.
568 Marlin BJ, Froemke RC (2017) Oxytocin modulation of neural circuits for social behavior. Dev

Neurobiol 77:169–189.

Marlin BJ, Mitre M, D'Amour JA, Chao M V, Froemke RC (2015) Oxytocin enables maternal behaviour by balancing cortical inhibition. Nature 520:499–504.

McRae BR, Andreu V, Marlin BJ (2023) Integration of olfactory and auditory cues eliciting parental behavior. J Neuroendocrinol:1–11.

Meijer GT, Mertens PEC, Pennartz CMA, Olcese U, Lansink CS (2019) The circuit architecture of cortical multisensory processing: Distinct functions jointly operating within a common anatomical network. Prog Neurobiol 174:1–15 Available at: https://doi.org/10.1016/j.pneurobio.2019.01.004.

Meijer GT, Montijn JS, Pennartz CMA, Lansink CS (2017) Audiovisual modulation in mouse primary visual cortex depends on cross-modal stimulus configuration and congruency. J Neurosci 37:8783–8796.

Meijer GT, Pie JL, Dolman TL, Pennartz CMA, Lansink CS (2018) Audiovisual integration enhances stimulus detection performance in mice. Front Behav Neurosci 12:231 Available at: https://www.frontiersin.org/article/10.3389/fnbeh.2018.00231/full [Accessed November 18, 2020].

Olofsson JK, Zhou G, East BS, Zelano C, Wilson DA (2019) Odor identification in rats: Behavioral and electrophysiological evidence of learned olfactory-auditory associations. eNeuro 6 Available at: https://doi.org/10.1523/ENEURO.0102-19.2019 [Accessed July 1, 2020].

Pachitariu M, Steinmetz N, Kadir S, Carandini M, Harris KD (2016) Kilosort: realtime spike-sorting for extracellular electrophysiology with hundreds of channels. bioRxiv:061481 Available at: http://biorxiv.org/lookup/doi/10.1101/061481.

Seo H-S, Hummel T (2011) Auditory-Olfactory Integration: Congruent or Pleasant Sounds Amplify Odor Pleasantness. Chem Senses 36:301–309 Available at: https://academic.oup.com/chemse/article/36/3/301/506704 [Accessed November 24,

2020].

Seo H-S, Lohse F, Luckett CR, Hummel T (2014) Congruent Sound Can Modulate Odor Pleasantness. Chem Senses 39:215–228 Available at: https://academic.oup.com/chemse/article/39/3/215/502704 [Accessed November 24, 2020].

Shepherd GMG (2013) Corticostriatal connectivity and its role in disease. Nat Rev Neurosci 14:278–291 Available at: www.nature.com/reviews/neuro [Accessed October 15, 2020].

Shusterman R, Smear MC, Koulakov AA, Rinberg D (2011) Precise olfactory responses tile the sniff cycle. Nat Neurosci 14:1039–1044.

Siegle JH, López AC, Patel YA, Abramov K, Ohayon S, Voigts J (2017) Open Ephys: An open-source, plugin-based platform for multichannel electrophysiology. J Neural Eng 14.

Smith JJ, Shionoya K, Sullivan RM, Wilson DA (2009) Auditory stimulation dishabituates olfactory responses via noradrenergic cortical modulation. Neural Plast 2009.

Tasaka G ichi, Feigin L, Maor I, Groysman M, DeNardo LA, Schiavo JK, Froemke RC, Luo L, Mizrahi A (2020) The Temporal Association Cortex Plays a Key Role in Auditory-Driven Maternal Plasticity. Neuron 107:566-579.e7 Available at: https://doi.org/10.1016/j.neuron.2020.05.004.

Tasaka G ichi, Maggi C, Taha E, Mizrahi A (2023) The local and long-range input landscape of inhibitory neurons in mouse auditory cortex. J Comp Neurol 531:502–514.

Varga AG, Wesson DW (2013) Distributed auditory sensory input within the mouse olfactory cortex. Eur J Neurosci 37:564–571.

Wallace MT, Woynaroski TG, Stevenson RA (2020) Multisensory integration as a window into orderly and disrupted cognition and communication. Annu Rev Psychol 71:193–219 Available at: https://doi.org/10.1146/annurev-psych-010419- [Accessed November 20, 2020].

Wesson DW, Wilson DA (2010) Smelling sounds: Olfactory-auditory sensory convergence in the

621 olfactory tubercle. J Neurosci 30:3013–3021.
622 Wesson DW, Wilson DA (2011) Sniffing out the contributions of the olfactory tubercle to the
623 sense of smell: Hedonics, sensory integration, and more? Neurosci Biobehav Rev 35:655–
624 668 Available at: http://dx.doi.org/10.1016/j.neubiorev.2010.08.004.
625 Williams E, Dewan A (2020) Olfactory detection thresholds for primary aliphatic alcohols in
626 mice. Chem Senses 45:513–521.
627 Wu T, Li S, Du D, Li R, Liu P, Yin Z, Zhang H, Qiao Y, Li A (2023) Olfactory–auditory sensory
628 integration in the lateral entorhinal cortex. Prog Neurobiol 221:102399 Available at:
629 https://doi.org/10.1016/j.pneurobio.2022.102399.
630 Zelano C, Mohanty A, Gottfried JA (2011) Olfactory Predictive Codes and Stimulus Templates
631 in Piriform Cortex. Neuron 72:178–187 Available at:
632 http://dx.doi.org/10.1016/j.neuron.2011.08.010.
633 Zhou H yu, Cheung EFC, Chan RCK (2020) Audiovisual temporal integration: Cognitive
634 processing, neural mechanisms, developmental trajectory and potential interventions.
635 Neuropsychologia 140 Available at:
636 https://doi.org/10.1016/j.neuropsychologia.2020.107396 [Accessed November 20, 2020].
637 Zingg B, Peng B, Huang J, Tao HW, Zhang LI (2020) Synaptic specificity and application of
638 anterograde transsynaptic AAV for probing neural circuitry. J Neurosci 40:3250–3267
639 Available at: https://doi.org/10.1523/JNEUROSCI.2158-19.2020 [Accessed October 15,
640 2020].
641

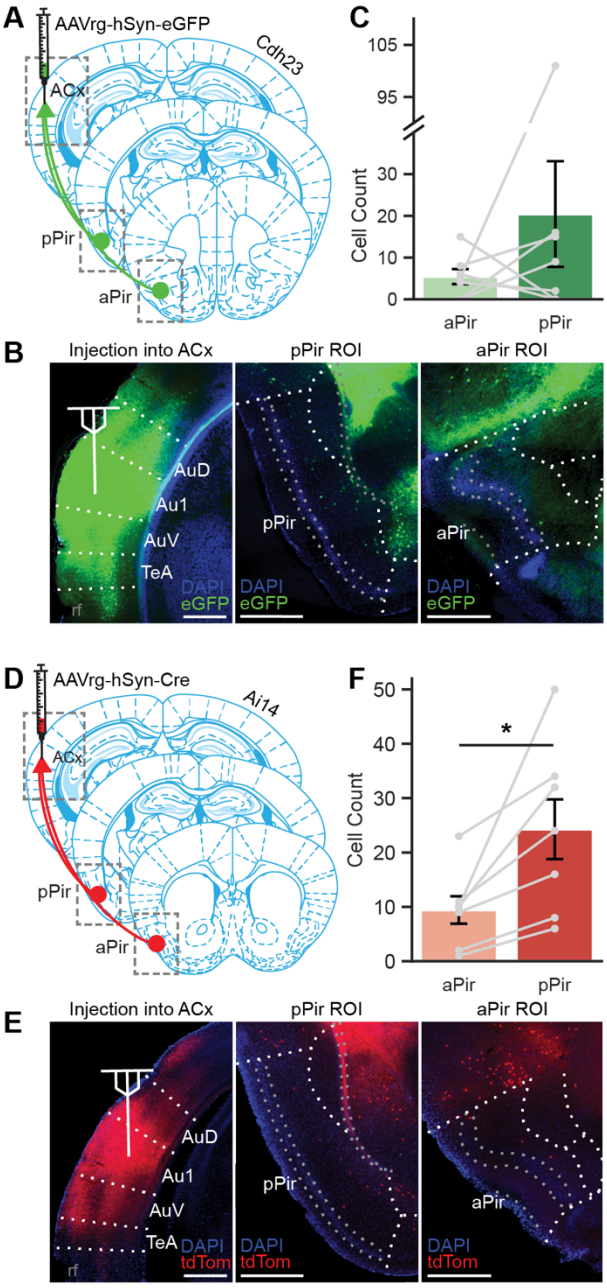

Figure 1. Neurons in the ipsilateral piriform cortex directly project to the auditory cortex. **A)** Injection of AAVrg-hSyn-eGFP into the left auditory cortex (ACx) of Cdh23 mice. **B)** Representative fluorescent micrographs of ACx injection site (left), posterior piriform (pPir) ROI (middle), anterior piriform (aPir) ROI (right). Scale bars = 500 µm. **C)** Number of cells labeled with GFP in aPir and pPir (n=7 mice; n.s. p=0.375, Wilcoxon signed-rank test). **D)** Injection of AAVrg-hSyn-Cre into the left ACx of Ai14 mice. **E)** Representative fluorescent micrographs of ACx

649 injection site (left), pPir ROI (middle), aPir ROI (right). Scale bars = 500 μm. **F)** Number of cells

650 labeled with tdTomato in aPir and pPir (n=7 mice; *p=0.020, paired t-test).

651

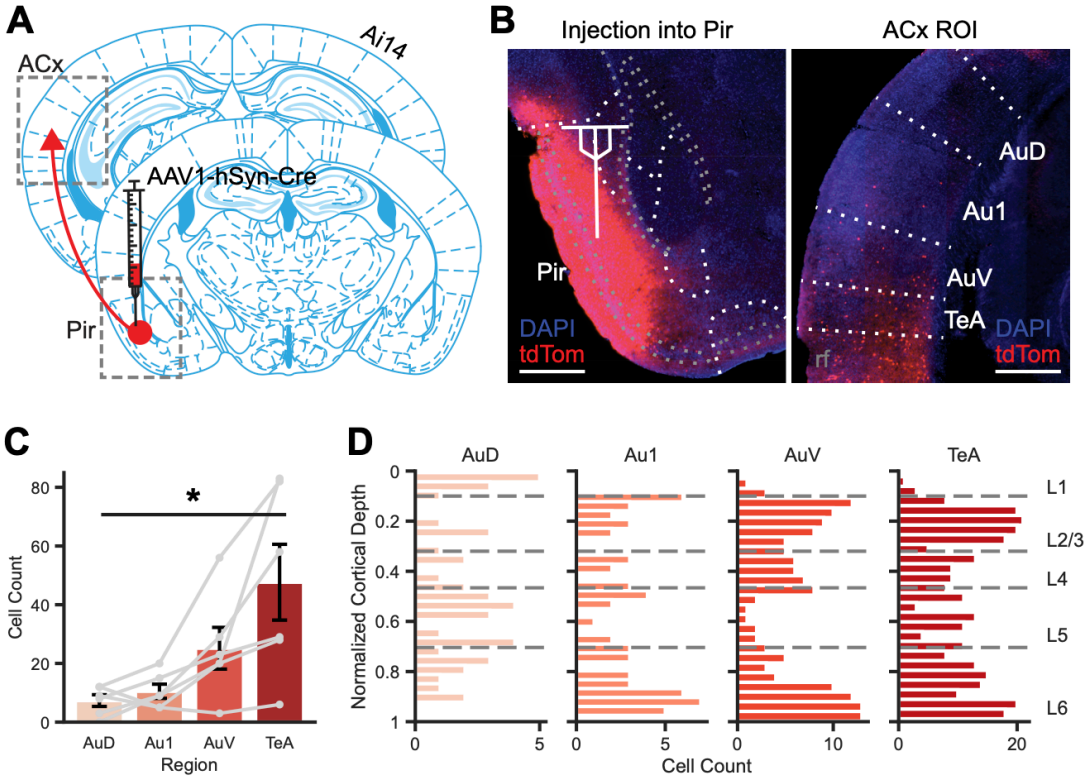

Figure 2. Neurons that receive piriform cortical input span auditory cortical regions. A) Injection of AAV1-hSyn-Cre into the left piriform cortex (Pir) of Ai14 mice. **B)** Representative fluorescent micrographs of the Pir injection site (left) and auditory cortical ROIs (right). Scale bars = 500 μm. **C)** Number of cells labeled with tdTomato across auditory cortical regions (n=6 mice; *p=0.0141, Friedman test). **D)** Histograms of the depth distribution of labeled cells in each auditory cortical region (all cells from 6 mice).

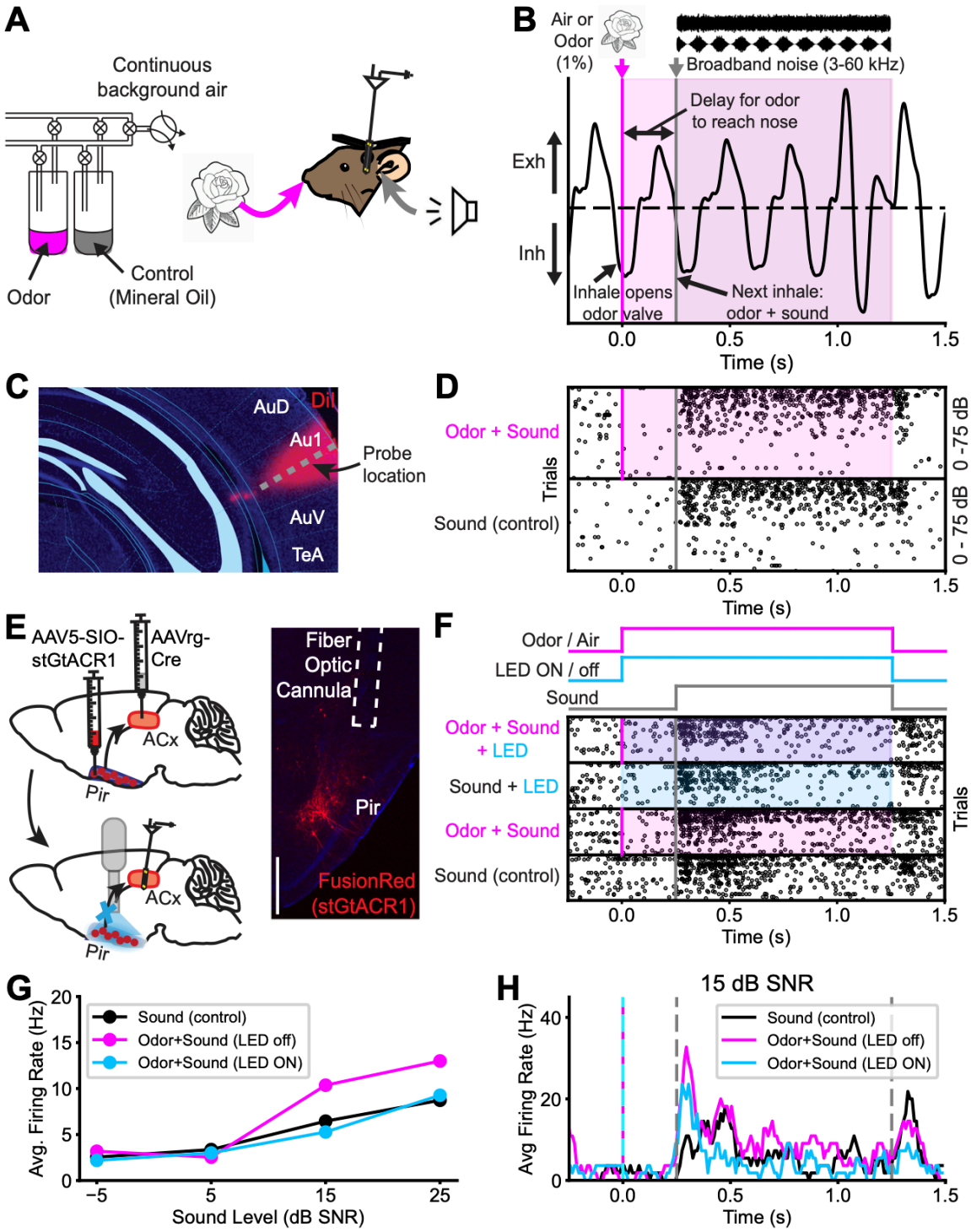

Figure 3. *In vivo* electrophysiology for assessing auditory-olfactory integration in auditory cortex. A) Experimental setup for delivering combinations of odor/sounds to awake mice during recordings. **B)** Stimulus timing using respiration-triggered olfactometer. **C)** Example post-hoc

663 visualization of probe location using DiI. **D)** Example raster plot from sound-responsive ACx unit.
664 Trials sorted by sound intensity and odor/control**. E)** Virus injections for selectively expressing
665 stGtACR1 in ACx-projecting Pir neurons. Right: example opsin expression in Pir and cannula
666 placement for in vivo optogenetics using 470 nm LED. **F)** Stimulus timing during optogenetic
667 experiments and example raster plot from ACx unit. Trials sorted by sound intensity and odor/LED
668 combination. **G)** Average firing rates (Hz) of example unit shown in F, in response to various sound
669 levels (dB SNR relative to background noise of olfactometer air flow) in control and odor, with and
670 without LED inactivation of PCx-to-ACx projections. **H)** Peristimulus time histogram (PSTH) of
671 example unit shown in F and G, in response to 15 dB SNR sound.
672

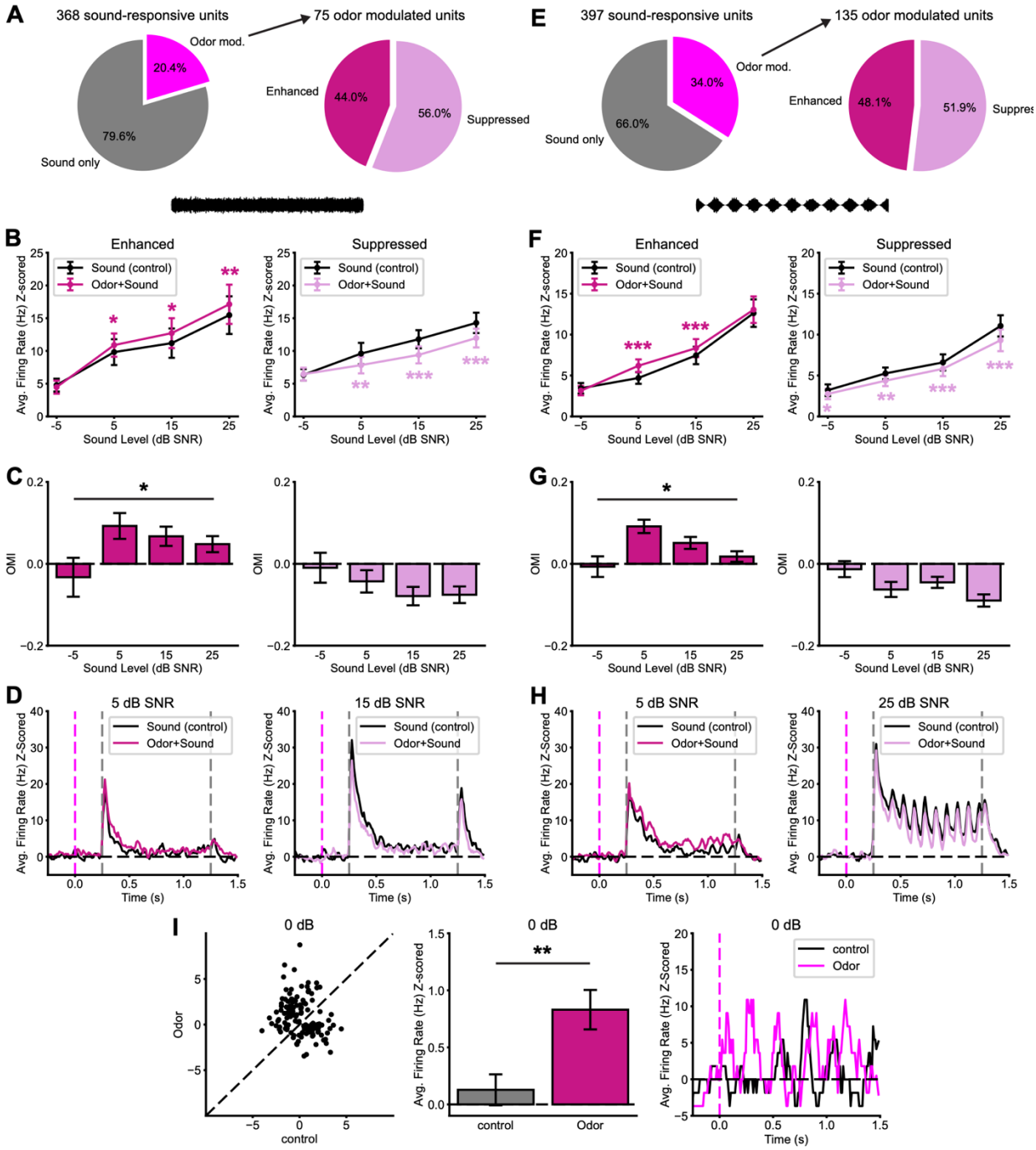

Figure 4. Odor modulates sound responses in auditory cortex. A) Left: Percentage of significantly odor-modulated units in ACx in response to unmodulated broadband noise, according to GLM. Right: percentage of Enhanced vs Suppressed odor-modulated units. n=5 mice, 368 sound-responsive units, 293 'Sound only' units, 75 'Odor mod.' units, 33 Enhanced units, 42

Suppressed units. **B)** Average responses to sound levels (dB SNR relative to noise of background air flow), with Odor versus control, for Enhanced units (left) and Suppressed units (right). *p<0.05, **p<0.01, ***p<0.001, Wilcoxon signed-rank tests. **C)** Average Odor Modulation Index (OMI) for each sound level, for Enhanced units (left) and Suppressed units (right). *p<0.05, Friedman test. **D)** Average PSTHs in response to 5 dB SNR (left) and 15 dB SNR (right) sound. Dashed magenta line indicates odor valve opening time, gray lines indicate sound stimulus start and stop times. **E-H)** Same as A-D, for 10 Hz amplitude modulated noise. n= 5 mice, 397 sound-responsive units, 262 'Sound only' units, 135 'Odor mod.' units, 65 Enhanced units, 70 Suppressed units. **F)** *p<0.05, **p<0.01, ***p<0.001, Wilcoxon signed-rank tests. **G)** *p<0.05, Friedman test. **I)** Left and middle: Average firing rate (z-scored) for odor-modulated units (10 Hz AM; units in E, n=135 units), in response to Odor versus control, in the absence of sound (0 dB). **p<0.01, Wilcoxon signed-rank test. Right: PSTH from an example odor-modulated unit, in the absence of sound (0 dB).

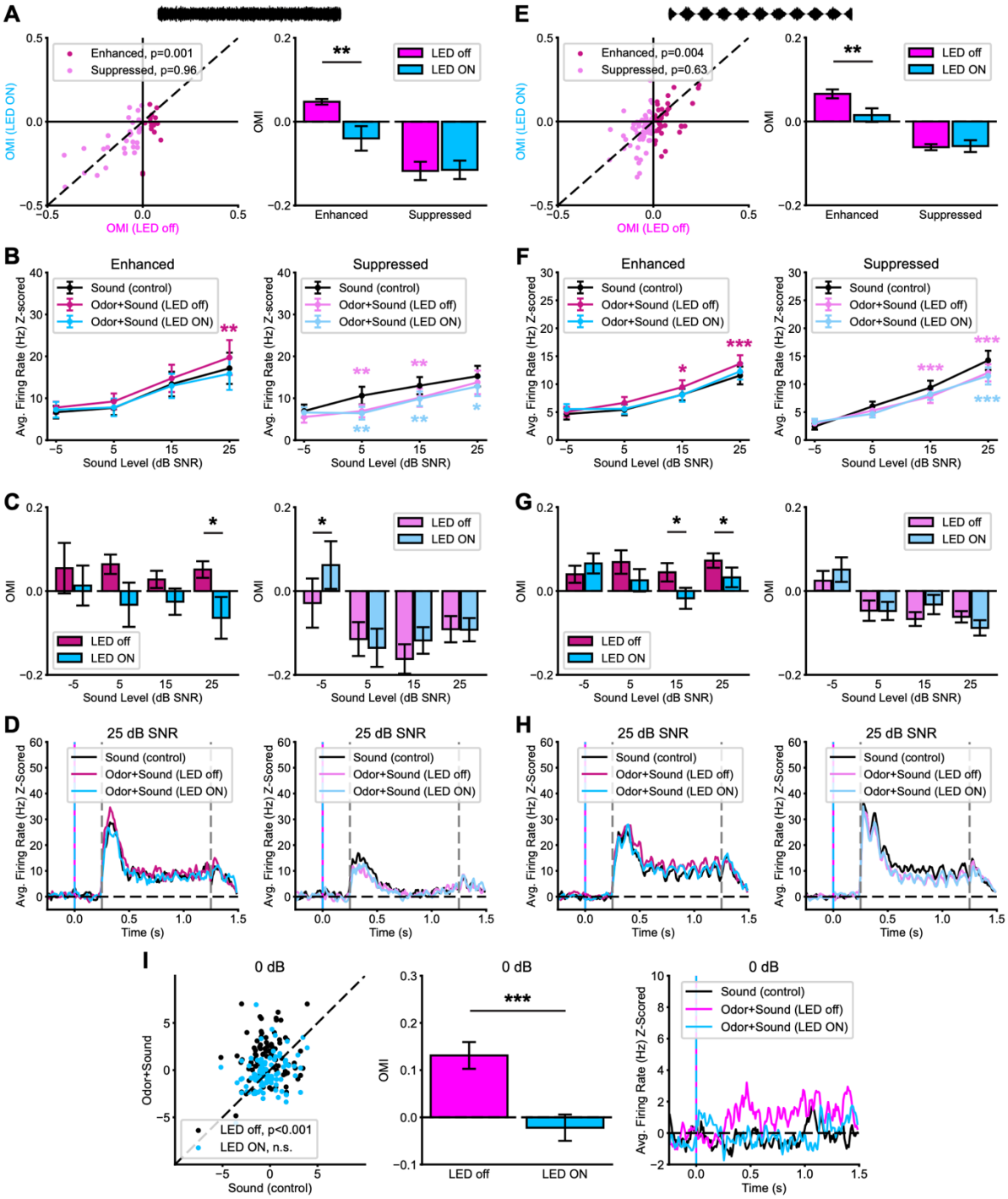

Figure 5. *In vivo* optogenetic inactivation of ACx-projecting piriform neurons reduces odor-mediated enhancement but not suppression. A) Left: Odor Modulation Index (OMI) with vs without LED, for Enhanced and Suppressed ACx units in response to unmodulated broadband

694 noise. n= 6 mice, 16 Enhanced units, 29 Suppressed units. Wilcoxon signed-rank tests LED off
695 vs LED ON. Right: Average OMI for Enhanced and Suppressed units, LED off vs LED ON.
696 **p<0.01, Wilcoxon signed-rank test. **B)** Average responses to various sound levels (dB SNR
697 relative to noise of background air flow): sound alone versus odor with or without LED, for
698 Enhanced units (left) and Suppressed units (right). *p<0.05, **p<0.01, Wilcoxon signed-rank tests
699 vs. 'Sound (control)'. **C)** Average OMI for each sound level, for Enhanced units (left) and
700 Suppressed units (right). *p<0.05, Wilcoxon signed-rank test. **D)** Average PSTHs in response to
701 25 dB SNR sound stimulus. Dashed magenta and cyan lines indicate odor valve opening and
702 LED ON time, gray lines indicate sound stimulus start and stop times. **E-H)** Same as A-D, for 10
703 Hz amplitude modulated noise. n= 6 mice, 37 Enhanced units, 54 Suppressed units. E) **p<0.01,
704 Wilcoxon signed-rank test. **F)** *p<0.05, ***p<0.001, Wilcoxon signed-rank tests vs. 'Sound
705 (control)' **G)** *p<0.05, Wilcoxon signed-rank tests. **I)** Left: Average firing rate (z-scored) for odor
706 modulated units (10 Hz AM; units in E, n=91 units) in the absence of sound (0 dB), in response
707 to Odor versus control with LED off and LED ON. LED off: ***p<0.0001, paired t-test. LED ON:
708 n.s. p>1, Wilcoxon signed-rank test. Middle: Average OMI in the absence of sound (0 dB), LED
709 off vs LED ON, ***p<0.001, Wilcoxon signed-rank test. Right: Average PSTH for odor-modulated
710 units, in the absence of sound (0 dB).

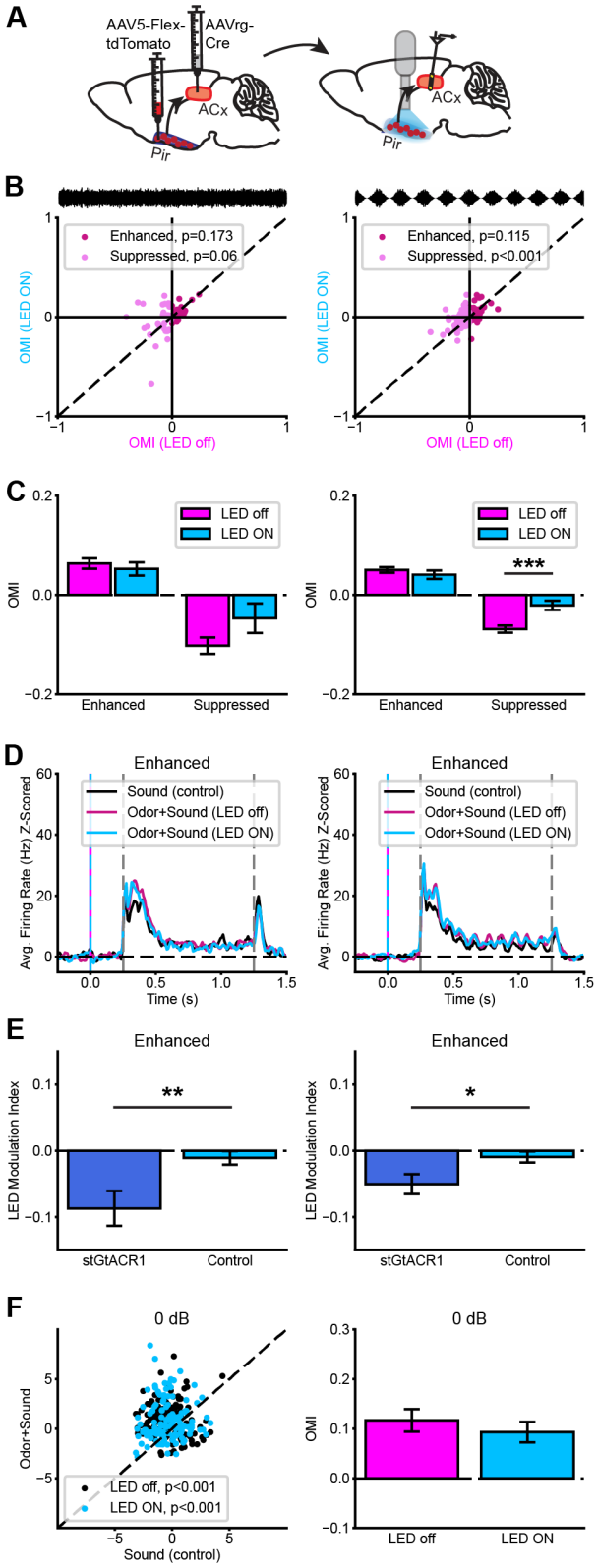

Figure 6. Optogenetic inhibition of odor-mediated enhancement is specifically due to inactivation of ACx-projecting Pir neurons. A) Virus injections for optogenetic control

714 experiments expressing control virus in ACx-projecting Pir neurons. **B)** Left: OMI with vs without
715 LED, for Enhanced and Suppressed ACx units in response to unmodulated broadband noise. n=
716 7 mice, 26 Enhanced units, 32 Suppressed units. Wilcoxon signed-rank tests LED off vs LED ON.
717 Right: Same as Left, but in response to 10 Hz AM noise. n= 7 mice, 60 Enhanced units, 72
718 Suppressed units. Wilcoxon signed-rank tests LED off vs LED ON. **C)** Average OMI for Enhanced
719 and Suppressed units, LED off vs LED ON., in response to unmodulated noise (left) and 10 Hz
720 AM noise (right). ***p<0.001, Wilcoxon signed-rank test. **D)** Average PSTHs in response to 25 dB
721 SNR sound, for unmodulated (left) and 10 Hz AM noise (right). **E)** LED Modulation Index for
722 Enhanced units in response to unmodulated (left) and 10 Hz AM (right) noise, in stGtACR1 mice
723 versus Control mice. Left: stGtACR1: n=16 units; Control: n=26 units; **p<0.01, Mann-Whitney
724 test. Right: stGtACR1: n=37 units; Control: n=60 units; *p<0.05, Mann-Whitney test. **F)** Left:
725 Average firing rate (z-scored) for odor-modulated units (10 Hz AM; units in B, right, n=132 units)
726 in the absence of sound (0 dB), in response to Odor versus control with LED off and LED ON.
727 LED off: ***p<0.0001, paired t-test. LED ON: ***p<0.0001, Wilcoxon signed-rank test. Right:
728 Average OMI in the absence of sound (0 dB), LED off vs LED ON. n.s. Wilcoxon signed-rank test.
729
730
731

732 **Table 1. Statistical comparisons.** Detailed values and statistical tests for all data figures.

733

Figure	Comparison	Test	n	Test statistic	p-value	Bonferroni corrected p-value
1C	Cell count, aPir vs. pPir	Wilcoxon signed-rank test	7 mice	W = 8	0.38	
1F	Cell count, aPir vs. pPir	Paired t-test	7 mice	t = -3.14	0.020	
2C	Cell count, by Region	Friedman test	6 mice	Q = 10.6	0.014	
4B, left	Enhanced: -5 dB SNR: Sound (control) vs. Odor+Sound	Wilcoxon signed-rank test	33 units	W = 235	0.59	
	Enhanced: 5 dB SNR: Sound (control) vs. Odor+Sound			W = 130.5	0.013	
	Enhanced: 15 dB SNR: Sound (control) vs. Odor+Sound			W = 154	0.023	
	Enhanced: 25 dB SNR: Sound (control) vs. Odor+Sound			W = 127	0.0093	
4B, right	Suppressed: -5 dB SNR: Sound (control) vs. Odor+Sound	Wilcoxon signed-rank test	42 units	W = 357	0.65	
	Suppressed: 5 dB SNR: Sound (control) vs. Odor+Sound			W = 219	0.0061	
	Suppressed: 15 dB SNR: Sound (control) vs. Odor+Sound			W = 128	0.00015	
	Suppressed: 25 dB SNR: Sound (control) vs. Odor+Sound			W = 159	0.00043	
4C, left	Enhanced: OMI, by Sound Level	Friedman test	33 units	Q = 8.36	0.039	
4C, right	Suppressed: OMI, by Sound Level	Friedman test	42 units	Q = 3.46	0.33	
4F, left	Enhanced: -5 dB SNR: Sound (control) vs. Odor+Sound	Wilcoxon signed-rank test	65 units	W = 983	0.56	
	Enhanced: 5 dB SNR: Sound (control) vs. Odor+Sound			W = 373	8.2e-6	
	Enhanced: 15 dB SNR: Sound (control) vs. Odor+Sound			W = 531	0.0004	

	Enhanced: 25 dB SNR: Sound (control) vs. Odor+Sound			W = 789	0.064	
4F, right	Suppressed: -5 dB SNR: Sound (control) vs. Odor+Sound	Wilcoxon signed-rank test	70 units	W = 819	0.013	
	Suppressed: 5 dB SNR: Sound (control) vs. Odor+Sound			W = 642	0.0012	
	Suppressed: 15 dB SNR: Sound (control) vs. Odor+Sound			W = 661	0.0007	
	Suppressed: 25 dB SNR: Sound (control) vs. Odor+Sound			W = 354	2.0e-7	
4G, left	Enhanced: OMI, by Sound Level	Friedman test	65 units	Q = 9.13	0.028	
4G, right	Suppressed: OMI, by Sound Level	Friedman test	70 units	Q = 3.88	0.27	
4I	Firing Rate, control vs. Odor	Wilcoxon signed-rank test	135 units	W = 3286	0.0042	
5A	Enhanced: OMI (LED off) vs. OMI (LED ON)	Wilcoxon signed-rank test	16 units	W = 9	0.001	
5A	Suppressed: OMI (LED off) vs. OMI (LED ON)		29 units	W = 201	0.96	
5B, left	Enhanced: -5 dB SNR: Sound (control) vs. Odor+Sound (LED off)	Paired t-test	16 units	t = -1.14	0.27	0.54
	Enhanced: 5 dB SNR: Sound (control) vs. Odor+Sound (LED off)			t = -1.85	0.085	0.17
	Enhanced: 15 dB SNR: Sound (control) vs. Odor+Sound (LED off)	Wilcoxon signed-rank test		W = 28	0.069	0.14
	Enhanced: 25 dB SNR: Sound (control) vs. Odor+Sound (LED off)			W = 15	0.0042	0.0084
5B, left	Enhanced: -5 dB SNR: Sound (control) vs. Odor+Sound (LED ON)	Wilcoxon signed-rank test	16 units	W = 61	0.74	1.49
	Enhanced: 5 dB SNR: Sound (control) vs. Odor+Sound (LED ON)			W = 62	0.78	1.56
	Enhanced: 15 dB SNR: Sound (control) vs. Odor+Sound (LED ON)			W = 52	0.43	0.87
	Enhanced: 25 dB SNR: Sound (control) vs. Odor+Sound (LED ON)			W = 52	0.43	0.87

5B, right	Suppressed: -5 dB SNR: Sound (control) vs. Odor+Sound (LED off)	Wilcoxon signed-rank test	29 units	W = 155	0.18	0.37
	Suppressed: 5 dB SNR: Sound (control) vs. Odor+Sound (LED off)			W = 53	0.0006	0.0012
	Suppressed: 15 dB SNR: Sound (control) vs. Odor+Sound (LED off)			W = 47	0.0006	0.0012
	Suppressed: 25 dB SNR: Sound (control) vs. Odor+Sound (LED off)			W = 119	0.093	0.19
5B, right	Suppressed: -5 dB SNR: Sound (control) vs. Odor+Sound (LED ON)	Wilcoxon signed-rank test	29 units	W = 206	0.81	1.63
	Suppressed: 5 dB SNR: Sound (control) vs. Odor+Sound (LED ON)			W = 54	0.0007	0.0014
	Suppressed: 15 dB SNR: Sound (control) vs. Odor+Sound (LED ON)			W = 57	0.0009	0.0018
	Suppressed: 25 dB SNR: Sound (control) vs. Odor+Sound (LED ON)			W = 92	0.0056	0.011
5C, left	Enhanced: OMI -5 dB SNR: LED off vs. LED ON	Paired t-test	16 units	t = 1.30	0.21	
	Enhanced: OMI 5 dB SNR: LED off vs. LED ON	Wilcoxon signed-rank test		W = 47	0.30	
	Enhanced: OMI 15 dB SNR: LED off vs. LED ON	Paired t-test		t = 1.31	0.21	
	Enhanced: OMI 25 dB SNR: LED off vs. LED ON			t = 2.22	0.042	
5C, right	Suppressed: OMI -5 dB SNR: LED off vs. LED ON	Wilcoxon signed-rank test	29 units	W = 105	0.044	
	Suppressed: OMI 5 dB SNR: LED off vs. LED ON	Paired t-test		t = 0.49	0.63	
	Suppressed: OMI 15 dB SNR: LED off vs. LED ON	Wilcoxon signed-rank test		W = 171	0.33	
	Suppressed: OMI 25 dB SNR: LED off vs. LED ON			W = 188	0.73	
5E	Enhanced: OMI (LED off) vs. OMI (LED ON)	Wilcoxon signed-rank test	37 units	W = 165	0.0041	

5E	Suppressed: OMI (LED off) vs. OMI (LED ON)		54 units	W = 636	0.63	
5F, left	Enhanced: -5 dB SNR: Sound (control) vs. Odor+Sound (LED off)	Wilcoxon signed-rank test	37 units	W = 292	0.38	0.76
	Enhanced: 5 dB SNR: Sound (control) vs. Odor+Sound (LED off)			W = 210	0.053	0.11
	Enhanced: 15 dB SNR: Sound (control) vs. Odor+Sound (LED off)			W = 150	0.0069	0.014
	Enhanced: 25 dB SNR: Sound (control) vs. Odor+Sound (LED off)			W = 95	0.0002	0.0004
5F, left	Enhanced: -5 dB SNR: Sound (control) vs. Odor+Sound (LED ON)	Wilcoxon signed-rank test	37 units	W = 222	0.08	0.16
	Enhanced: 5 dB SNR: Sound (control) vs. Odor+Sound (LED ON)			W = 308	0.52	1.04
	Enhanced: 15 dB SNR: Sound (control) vs. Odor+Sound (LED ON)			W = 332	0.78	1.55
	Enhanced: 25 dB SNR: Sound (control) vs. Odor+Sound (LED ON)			W = 294	0.39	0.79
5F, right	Suppressed: -5 dB SNR: Sound (control) vs. Odor+Sound (LED off)	Wilcoxon signed-rank test	54 units	W = 514	0.11	0.22
	Suppressed: 5 dB SNR: Sound (control) vs. Odor+Sound (LED off)			W = 490	0.03	0.06
	Suppressed: 15 dB SNR: Sound (control) vs. Odor+Sound (LED off)			W = 229	1.7e-5	3.3e-5
	Suppressed: 25 dB SNR: Sound (control) vs. Odor+Sound (LED off)			W = 243	1.7e-5	3.4e-5
5F, right	Suppressed: -5 dB SNR: Sound (control) vs. Odor+Sound (LED ON)	Wilcoxon signed-rank test	54 units	W = 490	0.03	0.059
	Suppressed: 5 dB SNR: Sound (control) vs. Odor+Sound (LED ON)			W = 484	0.026	0.052
	Suppressed: 15 dB SNR: Sound (control) vs. Odor+Sound (LED ON)			W = 525.5	0.06	0.12
	Suppressed: 25 dB SNR: Sound (control) vs. Odor+Sound (LED ON)			W = 220	6.8e-6	1.4e-5

5G, left	Enhanced: OMI -5 dB SNR: LED off vs. LED ON	Wilcoxon signed-rank test	37 units	W = 249	0.19	
	Enhanced: OMI 5 dB SNR: LED off vs. LED ON	Paired t-test		t = 1.69	0.11	
	Enhanced: OMI 15 dB SNR: LED off vs. LED ON	Wilcoxon signed-rank test		W = 188	0.013	
	Enhanced: OMI 25 dB SNR: LED off vs. LED ON			W = 199	0.021	
5G, right	Suppressed: OMI -5 dB SNR: LED off vs. LED ON	Wilcoxon signed-rank test	54 units	W = 726	0.89	
	Suppressed: OMI 5 dB SNR: LED off vs. LED ON			W = 710	0.96	
	Suppressed: OMI 15 dB SNR: LED off vs. LED ON			W = 553	0.10	
	Suppressed: OMI 25 dB SNR: LED off vs. LED ON	Paired t-test		t = 1.23	0.26	
5I, left	Firing Rate, control vs. Odor (LED off)	Paired t-test	91 units	t = -5.70	1.5e-7	3.1e-7
5I, left	Firing Rate, control vs. Odor (LED ON)	Wilcoxon signed-rank test		W = 1957	0.59	1.18
5I, middle	OMI, LED off vs. LED ON	Wilcoxon signed-rank test	91 units	W = 786	2.3e-7	
6B-C, left	Enhanced: OMI (LED off) vs. OMI (LED ON)	Wilcoxon signed-rank test	26 units	W = 121	0.17	
6B-C, left	Suppressed: OMI (LED off) vs. OMI (LED ON)		32 units	W = 152	0.06	
6B-C, right	Enhanced: OMI (LED off) vs. OMI (LED ON)	Wilcoxon signed-rank test	60 units	W = 676	0.11	
6B-C, right	Suppressed: OMI (LED off) vs. OMI (LED ON)		72 units	W = 487	7.6e-6	
6E, left	LED Modulation Index, stGtACR1 vs. Control	Mann-Whitney test	16 units; 26 units	U = 108	0.001	
6E, right	LED Modulation Index, stGtACR1 vs. Control	Mann-Whitney test	37 units; 60 units	U = 828	0.037	
6F, left	Firing Rate, control vs. Odor (LED off)	Paired t-test	132 units	t = -6.29	4.3e-9	8.7e-9

6F, left	Firing Rate, control vs. Odor (LED ON)	Wilcoxon signed-rank test		W = 2218	8.2e-7	1.6e-6
6F, right	OMI, LED off vs. LED ON	Wilcoxon signed-rank test	132 units	W = 3882	0.31	